Journal of Computational Physics **150,** 268–286 (1999)
Article ID jcph.1998.6180, available online at http://www.idealibrary.com on IDEAL®

AUSM(ALE): A Geometrically Conservative Arbitrary Lagrangian–Eulerian Flux Splitting Scheme

Richard W. Smith

Naval Surface Warfare Center, Coastal System Station, Panama City, Florida 32407
E-mail: smithr@atcf.ncsc.navy.mil

Received July 14, 1998; revised November 5, 1998

A geometrically conservative one-dimensional (1D) arbitrary Lagrangian–Eulerian (ALE) version of the advective upstream splitting method (AUSM) shock capturing scheme is presented. The spatial discretization is based on a modified form of AUSM which splits the flux vector according to the eigenvalues of the compressible Euler system in ALE form and recovers the original flux vector splitting in the absence of grid movement. The generalized form of AUSM is given the name AUSM(ALE). Extension to second-order accuracy is achieved by a piecewise linear reconstruction of the dependent variables with total variation diminishing limiting of slopes. The ALE formulation is completed by incorporating an implicit time-averaged normals form of the geometric conservation law for cylindrically and spherically symmetric time-dependent finite volumes which is valid for any two-level time-integration method. The effectiveness of the method for both fixed and moving grids is demonstrated via several 1D test problems including a standard shock tube problem and an infinite strength reflected shock problem. The method is then applied to a benchmark spherically symmetric underwater explosion problem to demonstrate the efficacy of the numerical procedure for problems of this type. In the two-phase detonation problem the spherical surface separating the expanding detonation-products gas bubble and the surrounding water is explicitly tracked as a Lagrangian surface using AUSM(ALE) in conjunction with appropriate equations of state describing the detonation-products gas and water phases. The basic features of the spherically symmetric detonation problem are discussed such as shock/free-surface interaction and late time hydrodynamics.

Key Words: flux splitting; arbitrary Lagrangian–Eulerian; geometric conservation law; underwater explosions.

0021-9991/99

INTRODUCTION

One class of problems in computational fluid dynamics that has undergone substantial development over the last decade is that in which the fluid domain boundary is either time dependent or unknown a priori and determined as part of the solution [1, 2]. Free-surface and fluid/structure interaction problems are typical of problems in this class [3, 4]. A natural way to formulate moving boundary problems is the so-called arbitrary Lagrangian–Eulerian (ALE) form of the fluid dynamic conservation laws where the domain boundary and interior control surfaces are allowed to move arbitrarily in time and which recovers the Eulerian and Lagrangian forms as special limiting cases of the general ALE form [5]. When the conservation laws admit discontinuous solutions, i.e., shocks and contacts, special care must be taken in the prescription of the numerical flux to ensure monotonicity and sharp resolution of discontinuities. Over the past decade characteristic-based upwind methods have established themselves as the methods of choice for prescribing the numerical flux function in shock capturing schemes [6]. Such methods are typically first order in their basic form with higher order accuracy achieved through reconstruction of primitive variables under a monotonicity principle such as total variation diminishing (TVD).

Upwind methods may generally be classified as either flux difference splitting (FDS) or flux vector splitting (FVS) schemes, with the methods of Roe [7] and Van Leer [8], respectively, being popular representatives of the two approaches. A recently developed scheme of the Van Leer type which can arguably be thought of as a natural candidate for ALE formulations is the advective upstream splitting method (AUSM) [9–11]. In this scheme the numerical interface flux of the Euler equations is parsed into convective and pressure contributions as required by the ALE form of the conservation laws. The AUSM-based ALE scheme presented here is particularly well suited to applications involving real fluid state equations and is offered as an alternative to the ALE scheme based on Roe's approximate Riemann solver for ideal gas flows [12].

ALE FORM OF THE COMPRESSIBLE EULER EQUATIONS

The equations governing inviscid compressible flow in the absence of heat conduction stated in weak or finite volume form are [13, 14]

$$\frac{\partial}{\partial t}\int_{\Omega(t)} W\,d\Omega + \oint_{\Gamma(t)} F(U, \boldsymbol{n}, \boldsymbol{s})\,d\Gamma = 0, \tag{1}$$

where

$$W = [\rho, \rho\boldsymbol{v}, \rho e_t]^T \qquad \text{and} \qquad F(W, \boldsymbol{n}, \boldsymbol{s}) = (\boldsymbol{v} - \boldsymbol{s}) \cdot \boldsymbol{n} W - [0, -p\boldsymbol{n}, -p\boldsymbol{v} \cdot \boldsymbol{n}]^T$$

or alternatively

$$F(W, \boldsymbol{n}, \boldsymbol{s}) = (\boldsymbol{v} - \boldsymbol{s}) \cdot \boldsymbol{n}[\rho, \rho\boldsymbol{v}, \rho h_t]^T - [0, -p\boldsymbol{n}, -p\boldsymbol{s} \cdot \boldsymbol{n}]^T.$$

In Eq. (1), W is the vector of conserved variables and F is the vector of inviscid flux components. The first term in the flux vector is the convective flux of the conserved variables through the time-dependent control surface Γ with outward unit normal $\boldsymbol{n}$. The second term is the vector of source terms which, for inviscid flows, contains only the pressure acting

and the work done on the control volume Ω. The fluid velocity vector, control surface velocity vector, fluid density, and pressure are given by $\boldsymbol{v}$, and $\boldsymbol{s}$, ρ, p, respectively. The alternative form of the flux vector is arrived at through the introduction of the total enthalpy, h_t. In Eq. (1), $\boldsymbol{s} = \boldsymbol{v}$ corresponds to the Lagrangian view of conservation whereas $\boldsymbol{s} = \boldsymbol{0}$ corresponds to the Eulerian view. Because of the generality or, in other words, arbitrariness of the description offered by Eq. (1) it is often referred to as the arbitrary Lagrangian–Eulerian form of the conservation laws.

In addition to the basic conservation laws expressed by Eq. (1) an equation of state (EOS) is necessary to provide closure to the Euler system and establish the relationship between, at most, three thermodynamic variables. Here the EOS is taken to be of the form

$$p = p(\rho, e), \tag{2a}$$

and the sound speed, c, can be determined from the state relation by

$$c^2 = \left.\frac{dp}{d\rho}\right|_s = \frac{\partial p}{\partial e}\frac{p}{\rho^2} + \frac{\partial p}{\partial p}. \tag{2b}$$

The internal energy, e, is related to the total energy by

$$e_t = e + \frac{|v|^2}{2}, \tag{3}$$

and the total enthalpy, h_t, which appears in the alternative form of the flux vector of Eq. (1), is defined as

$$h_t = e_t + \frac{p}{\rho}. \tag{4}$$

Equation (1) expresses the fundamental conservation laws for mass, momentum, and energy and is valid for any time-dependent finite volume of arbitrary shape. For the purpose at hand the flow is assumed to be one-dimensional (1D) and Eq. (1) is applied to the three finite volumes shown in Fig. 1, viz. a spherical arc volume, an annular arc volume, and a right hexahedron, associated with spherical, cylindrical, and Cartesian coordinate systems, respectively.

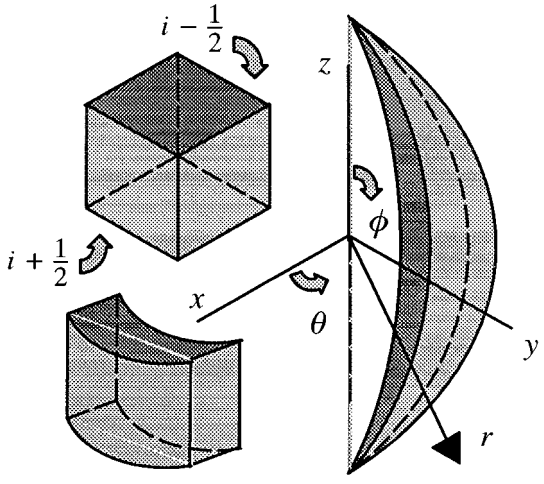

FIG. 1. Finite volumes used to develop 1D discrete form.

GEOMETRIC CONSERVATION LAW

Under certain assumptions regarding the flow field Eq. (1) reduces to a purely geometric statement relating the control volume $\Omega(t)$, the control surface $\Gamma(t)$, the control surface $\boldsymbol{s}(t)$, and the unit normal $\boldsymbol{n}(t)$. This statement is often referred to as the geometric conservation law (GCL), which may be regarded as an identity that must be satisfied, either explicitly or implicitly, if the conservative property is to be maintained [15]. Geometrically conservative formulas for general polygons and polyhedra used in finite volume schemes can be found in Zhang *et al.* [16] and Nkonga and Guillard [17]. A generalized treatment of the GCL is presented by Lesoinne and Farhat [18] which recovers the time-averaged normal formulas for polygons and polyhedra derived in [16, 17]. Owing to a particular interest in 1D radially symmetric flows, time-averaged normal formulas for the curvilinear finite volumes in Fig. 1 are derived here. For a broader treatment of the GCL for multi-dimensional problems the reader is referred to the aforementioned citations.

Although the continuity equation is typically used to derived the GCL any of the conservation laws expressed by Eq. (1) can be used with equal facility to derive the GCL under appropriate restrictions on the flow variables. Assuming uniform velocity and density fields and a closed control volume the continuity equation becomes

$$\frac{\partial \Omega}{\partial t} + \oint_{\Gamma(t)} (\boldsymbol{s} \cdot \boldsymbol{n})\, d\Gamma = 0. \tag{5}$$

Furthermore, assuming the control surface movement to be 1D and integrating over the control volume Eq. (5) reduces to the semi-discrete form

$$\frac{d\Omega_i}{dt} - (s\Gamma)_{i+1/2} + (s\Gamma)_{i-1/2} = 0. \tag{6}$$

Integrating Eq. (6) using a two-level time-integration scheme gives

$$\Omega_i^{n+1} - \Omega_i^n = \int_t^{t+\Delta t} [(s\Gamma)_{i+1/2} - (s\Gamma)_{i-1/2}]\, dt. \tag{7}$$

Equation (7) is a statement of geometric conservation and is a constraint which must be satisfied by any conservative two-level 1D finite volume scheme. It may be satisfied by updating $\Omega(t)$ through an explicit evaluation of Eq. (7) or implicitly by defining the control surface areas $\Gamma(t)$ as a weighted average of the n and $n+1$ time level areas such that Eq. (7) is satisfied exactly by construction.

As noted in [18], when the integrand of Eq. (7) is a linear function of t the integral can be computed exactly by sampling the integrand once at the midpoint of the interval. When the integrand is quadratic in t a two-point rule is required to evaluate the integral exactly. For the hexahedron, annular arc volume, and spherical arc volume shown in Fig. 1 the integrand in Eq. (7) is a zero-, first-, and second-degree polynomial in t, respectively. Consequently, for the finite volumes considered here, it is convenient to denote all GCL compliant time-averaged quantities as $n+1/2$ time-level quantities. Evaluating Eq. (7) at the midpoint of the time interval gives

$$\Omega_i^{n+1} - \Omega_i^n = \Delta t[(s\Gamma)_{i+1/2} - (s\Gamma)_{i-1/2}]^{n+1/2}, \tag{8}$$

where, following [18], the grid velocity is assumed to be constant over the time step and is given by

$$s_{i+1/2}^{n+1/2} = \frac{(x^{n+1} - x^n)_{i+1/2}}{\Delta t}. \tag{9}$$

Focusing on movement of the $i + 1/2$ face of the hexahedron in Fig. 1, the change in volume from time-level n to $n + 1$ is given by

$$\Omega_i^{n+1} - \Omega_i^n = (x^{n+1} - x^n)_{i+1/2}\, dy\, dz. \tag{10}$$

Equating Eqs. (8) and (10) gives

$$(x^{n+1} - x^n)_{i+1/2}\, dy\, dz = \Delta t\, (s\Gamma)_{i+1/2}^{n+1/2}. \tag{11}$$

Inspection of Eqs. (9) and (11) shows the GCL expressed by Eq. (7) to be trivially satisfied in the Cartesian case by

$$\Gamma_{i+1/2}^{n+1/2} = dy\, dz. \tag{12}$$

The situation for cylindrical and spherical coordinate systems is somewhat different since the integrand in Eq. (7) is no longer a constant. Specifically, the change in the annular arc control volume from time level n to $n + 1$ is given by

$$\Omega_i^{n+1} - \Omega_i^n = \frac{1}{2}((x^{n+1})^2 - (x^n)^2)_{i+1/2}\, d\theta\, dz, \tag{13}$$

where x is now a generic coordinate in the radial direction. Factoring the right-hand side of Eq. (13) and equating with Eq. (8) gives

$$\frac{1}{2}((x^{n+1} - x^n)(x^{n+1} + x^n))_{i+1/2}\, d\theta\, dz = \Delta t\, (s\Gamma)_{i+1/2}^{n+1/2}. \tag{14}$$

Inspection of Eqs. (9) and (14) shows the GCL is nontrivially satisfied in the cylindrical case by

$$\Gamma_{i+1/2}^{n+1/2} = \frac{1}{2}(x^{n+1} + x^n)_{i+1/2}\, d\theta\, dz. \tag{15}$$

For the spherical arc control volume the change in volume from time level n to $n + 1$ is given by

$$\Omega_i^{n+1} - \Omega_i^n = \frac{2}{3}((x^{n+1})^3 - (x^n)^3)_{i+1/2}\, d\theta \tag{16}$$

and again factoring the right-hand side of Eq. (16) and equating with Eq. (8) gives

$$\frac{2}{3}[(x^{n+1} - x^n)((x^{n+1})^2 + x^n x^{n+1} + (x^n)^2)]_{i+1/2}\, d\theta = \Delta t[s\Gamma]_{i+1/2}^{n+1/2}. \tag{17}$$

Inspection of Eqs. (9) and (17) shows the GCL is nontrivially satisfied in the spherical case by

$$\Gamma_{i+1/2}^{n+1/2} = \frac{2}{3}((x^{n+1})^2 + x^n x^{n+1} + (x^n)^2)_{i+1/2}\, d\theta. \tag{18}$$

From Eqs. (15) and (18) it can be seen that the control surface areas which implicitly satisfy the GCL are expressed as weighted averages of the areas at the n and $n+1$ time levels. The time-averaged formulas are summarized below for the three coordinate systems shown in Fig. 1. For completeness formulas are also given for the control volumes associated with each of the coordinate systems. In the following formulas the differential lengths and angles appearing in the above development have been set equal to one since they are arbitrary:

$$\Gamma_{i\pm1/2}^{n+1/2} = 1 \qquad \text{(Cartesian)}$$
$$\Omega_i^{n,n+1} = (x_{i+1/2} - x_{i-1/2})^{n,n+1} \tag{19a, 19b}$$

$$\Gamma_{i\pm1/2}^{n+1/2} = \frac{1}{2}(x^{n+1} + x^n)_{i\pm1/2} \qquad \text{(cylindrical)}$$
$$\Omega_i^{n,n+1} = \frac{1}{2}((x_{i+1/2} - x_{i-1/2})(x_{i+1/2} + x_{i-1/2}))^{n,n+1} \tag{20a, 20b}$$

$$\Gamma_{i\pm1/2}^{n+1/2} = \frac{2}{3}((x^{n+1})^2 + x^n x^{n+1} + (x^n)^2)_{i\pm1/2} \qquad \text{(spherical)}$$
$$\Omega_i^{n,n+1} = \frac{2}{3}\big((x_{i+1/2} - x_{i-1/2})\big((x_{i+1/2})^2 + x_{i+1/2}x_{i-1/2} + (x_{i-1/2})^2\big)\big)^{n,n+1}. \tag{21a, 21b}$$

The n, $n+1$ superscript appearing in the control volume formulas above indicate they are valid instantaneously at either the n or $n+1$ time level. Equations (19)–(21) have been verified to satisfy the GCL to machine precision for arbitrary grid movement. Consequently, no artifact due to grid motion is introduced in the solution of the conservation laws if these geometric relations are used in assembling the discrete form of Eq. (1). It may be noted that Eqs. (19)–(21) reduce to the standard geometric formulas for differential volumes and areas in the absence of grid motion.

THE INTERFACE FLUX

Although a number of characteristic-based upwind methods are available for spatially discretizing the compressible Euler equations (e.g., Roe's scheme [7], Godunov's method [19], etc.) AUSM has a number of attributes that make it particularly attractive in the context of an ALE formulation. More precisely, each member of the AUSM family of schemes (AUSM, AUSM$^+$, etc.) separates the pressure flux from the convective flux in the formulation of the basic scheme [9, 10]. This separation is essential to the ALE form of the conservation laws as seen in Eq. (1). In addition, AUSM can easily and simply accommodate general equations of state for real fluids since all that is required is the interrogation of the state relations for pressure and sound speed. Finally, the AUSM family of schemes are efficient and simple to implement compared to many popular and enduring schemes such as Godunov's method or Roe's scheme for real fluids [20].

The prescription for the interface flux in a FVS scheme is based on a decomposition or splitting of the flux vector into right and left travelling waves with the contribution of

each wave to the total flux determined by the local flow conditions in accordance with the eigenstructure of the Euler system. Typically, splitting is performed using the non-linear eigenvalues as the basis functions for developing second-degree polynomial splitting functions [6, 8].

In the absence of grid movement it is well known that the set of 1D Euler equations in strong quasi-linear form has eigenvalues [6]

$$\lambda_1 = u - c, \qquad \lambda_2 = u, \qquad \lambda_3 = u + c. \tag{22a}$$

In the presence of grid motion the same system can be shown to have modified eigenvalues

$$\hat{\lambda}_1 = \hat{u} - c, \qquad \hat{\lambda}_2 = \hat{u}, \qquad \hat{\lambda}_3 = \hat{u} + c, \tag{22b}$$

where $\hat{u}$ is simply the fluid velocity relative to the interface velocity, i.e., $\hat{u} = u - s$. Consequently, it is a rather simple step to construct splitting functions based on the ALE eigenvalues, Eq. (22b), as long as the separation of pressure and convection terms are maintained in the splitting as required by the ALE form. This is precisely the case with AUSM.

In what follows the ALE form of the U-split version of AUSM is presented. The resulting scheme is given the name AUSM(ALE). The scheme is developed in Cartesian coordinates for clarity with the final form valid for the three coordinate systems considered here. For 1D flows the semi-discrete form of Eq. (1) is given by

$$\frac{d}{dt}(W\Omega)_i + R_i = 0, \tag{23a}$$

where the residuals resulting from the spatial discretization are given by

$$R_i = [(F\Gamma)_{i+1/2} - (F\Gamma)_{i-1/2}]. \tag{23b}$$

The specific form of the ALE flux vector appearing in Eq. (23b) is not unique. Perhaps the most natural choice is given by

$$F = \hat{u} \begin{bmatrix} \rho \\ \rho u \\ \rho e_t \end{bmatrix} + \begin{bmatrix} 0 \\ p \\ pu \end{bmatrix}. \tag{24a}$$

This form [14] involves the work flux (pu) in the energy equation which can easily be computed as a product of the velocity and pressure splittings available in the U-split form of AUSM. However, numerical experiments with AUSM indicate the numerical flux based on Eq. (24a) results in a glitch at the downwind edge of the expansion wave for the Sod problem on a fixed grid.

An alternative ALE flux vector given in Eq. (1) is

$$F = \hat{u} \begin{bmatrix} \rho \\ \rho u \\ \rho h_t \end{bmatrix} + \begin{bmatrix} 0 \\ p \\ ps \end{bmatrix}. \tag{24b}$$

In this form the work flux is naturally accommodated by the introduction of the total enthalpy with the ALE flux vector recovering exactly the conventional flux vector in the

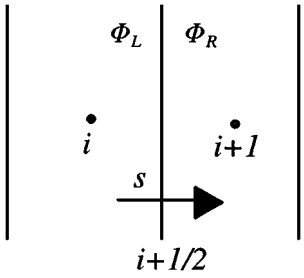

FIG. 2. Notation for interface flux at $i + 1/2$.

limit of zero grid velocity. As a result any flux splitting can be applied directly to the ALE flux vector, Eq. (24b), and have the original splitting recovered exactly on a fixed grid. Consequently, Eq. (24b) is considered to be the preferred ALE flux vector and is adopted for use in AUSM(ALE).

Finally, it should be pointed out that any member of the AUSM family of schemes can be applied to the ALE flux vector of Eq. (24b). For example, the M-split scheme AUSM$^+$ [10] has been recently extended to ALE form and applied to an aeroelastic problem involving transonic flow of an ideal gas [21]. Numerical experiments with other EOS have indicated the U-split version of AUSM to be somewhat more robust when used in conjunction with real fluid state equations, strong shocks and strong contact discontinuities such as those encountered in the application section of this paper. This is due in part to the fact that the U-split version is intrinsically more dissipative than the M-split versions [11]. Consequently, the U-split version is adopted here for the development of AUSM(ALE).

The U-split version of AUSM [11], when generalized to accommodate an interface moving with velocity s, gives the following prescription for the flux at the $i + 1/2$ interface separating states Φ_L and Φ_R as shown in Fig. 2,

$$F_{i+1/2} = \frac{1}{2}\left[\hat{u}_{i+1/2}(\Phi_L + \Phi_R) - |\hat{u}_{i+1/2}|(\Phi_R - \Phi_L)\right] + \begin{bmatrix} 0 \\ \hat{p} \\ ps \end{bmatrix}_{i+1/2}, \tag{25}$$

where in the 1D case

$$\Phi = [\rho, \rho u, \rho h_t]^T.$$

Here the fluid velocity relative to the moving interface is given by

$$\hat{u}_{i+1/2} = \hat{u}_L^+ + \hat{u}_R^-, \tag{26}$$

where

$$\hat{u}^{\pm} = \begin{cases} \pm\frac{1}{4c}(\hat{u} \pm c)^2 & \text{if } |\hat{u}| \le c \\ \frac{1}{2}(\hat{u} \pm |\hat{u}|) & \text{otherwise} \end{cases} \tag{27}$$

and

$$u_{i+1/2} = \hat{u}_L^+ + \hat{u}_R^- + s_{i+1/2}. \tag{28}$$

The pressure at the interface is given by

$$p_{i+1/2} = p_L^+ + p_R^-, \tag{29}$$

where

$$p^\pm = p\hat{u}^\pm \cdot \begin{cases} \frac{1}{c}\left(\pm 2 - \frac{\hat{u}}{c}\right) & \text{if } |\hat{u}| \le c \\ \frac{1}{\hat{u}} & \text{otherwise} \end{cases}. \tag{30}$$

In Eq. (25), $\hat{p}$ is introduced so that the homogeneous divergence form of Eq. (23) can be retained in cylindrical and spherical coordinates. The expressions for $\hat{p}$ are derived by reverting to the strong form of the momentum equation in cylindrical and spherical coordinates, assuming the pressure gradient to be constant and integrating over the control volume. This assumption is consistent with a spatially second-order accurate scheme. The expressions for $\hat{p}$ at the $i + 1/2$ interface are given below with similar expressions for $\hat{p}$ at the $i - 1/2$ interface:

$$\hat{p}_{i+1/2} = p_{i+1/2} \qquad \text{(Cartesian)} \tag{31}$$

$$\hat{p}_{i+1/2} = \frac{p_{i+1/2}}{2}\left(1 + \frac{x_{i-1/2}}{x_{i+1/2}}\right) \qquad \text{(cylindrical)} \tag{32}$$

$$\hat{p}_{i+1/2} = \frac{p_{i+1/2}}{3}\left[1 + \frac{x_{i-1/2}}{x_{i+1/2}} + \left(\frac{x_{i-1/2}}{x_{i+1/2}}\right)^2\right] \qquad \text{(spherical)}. \tag{33}$$

The prescription for the flux splitting in AUSM(ALE) can be seen in Eq. (27) and Eq. (30) to parse the flux based on the eigenvalues of the ALE form of the conservation laws and to reduce exactly to the fixed grid AUSM splitting in the absence of grid motion. Furthermore, it can be shown that the presence of the pressure flux (ps) in the ALE flux vector, Eq. (24b), does not alter the eigenvalues of the system beyond the modifications indicated in Eq. (22b). Consequently, AUSM(ALE) represents a generalization of the fixed grid U-split AUSM scheme. The performance of the scheme when used in conjunction with the geometrically conservative formulas (Eqs. (19)–(21)) will be tested in the following sections.

NUMERICAL FLUX AT A LAGRANGIAN INTERFACE

The utility of the ALE form lies in the fact that grid motion may be arbitrarily specified. The flexibility offered by arbitrary grid motion can be exploited to great advantage in a variety of circumstances. For example, if the fluid dynamics are forced or otherwise influenced by boundary motion, the boundary conditions can often be easily implemented by fixing the grid to the moving domain boundary. Alternatively, by appropriate definition of grid velocity a Lagrangian surface(s) can be established in the computational domain for the purpose of distinguishing and tracking material boundaries. By definition, a Lagrangian surface is established at a control surface by setting the interface velocity equal to the fluid velocity at the interface. This can be done wherever the fluid velocity is defined and continuous. After specifying the grid velocity at one point, for example, at a domain boundary or a contact surface, then it is usually a simple matter to construct a suitable (e.g., linear, exponential, etc.) distribution of grid velocity at all other points in the domain.

By definition, the convective flux vanishes at a Lagrangian surface. Inspection of Eq. (25) reveals that the dissipation term in AUSM(ALE) also vanishes there. Consequently, the only nonvanishing flux components at a Lagrangian surface are the pressure fluxes in the momentum and energy equations. In these circumstances it has been found that introducing a common speed of sound at the Lagrangian interface leads to an improvement in the performance of the scheme at the interface. A common speed of sound has also been used in the development of AUSM$^+$ and AUSMD/DV schemes to unify the velocity and Mach number splittings [10, 11]. The common sound speed c_m proposed in the AUSMD/DV scheme is adopted here and it is stressed that the common sound speed is introduced only at Lagrangian interfaces. The common sound speed is given by

$$c_m = \max(c_L, c_R). \tag{34}$$

EXTENSION TO SECOND-ORDER ACCURACY

In the previous section the L and R states at the $i+1/2$ interface were left unspecified. If these states are taken as the cell-averaged values in the adjoining control volumes the resulting scheme is spatially first-order accurate. Here second-order accuracy is achieved by a linear one-sided reconstruction of the state variables with TVD-based limiting of slopes [6]. Specifically, interface values of ρ, u, and e are reconstructed from the cell-centered values according to

$$(V_L)_{i+1/2} = V_i + \Psi(r_i)(V_i - V_{i-1})\left(\frac{\Delta x_i}{\Delta x_i + \Delta x_{i-1}}\right) \tag{35}$$

$$(V_R)_{i+1/2} = V_{i+1} - \Psi\left(\frac{1}{r_{i+1}}\right)(V_{i+2} - V_{i+1})\left(\frac{\Delta x_{i+1}}{\Delta x_{i+1} + \Delta x_{i+2}}\right), \tag{36}$$

where V is the vector of primitive variables $V = [\rho, u, e]^T$, r is the slope ratio, given by

$$r_i = \frac{(V_{i+1} - V_i)(\Delta x_i + \Delta x_{i-1})}{(V_i - V_{i-1})(\Delta x_i + \Delta x_{i+1})}, \tag{37}$$

and $\Psi(r)$ is the slope limiting function, and $\Delta x_i = x_i - x_{i-1}$. The minmod limiter is used in the present formulation [6].

TIME INTEGRATION

Equation (23) is supplemented by an auxiliary equation governing grid movement and the system is integrated in time using a 4-stage low-storage Runge–Kutta scheme [22]. The general m-stage scheme is given by

$$\tilde{W}^{(0)} = \tilde{W}^n \tag{38a}$$

$$\tilde{W}^{(k)} = \tilde{W}^n - a_k \Delta t \tilde{R}^{(k-1)}, \qquad k = 1, \ldots, m \tag{38b}$$

$$\tilde{W}^{n+1} = \tilde{W}^{(m)}, \tag{38c}$$

where the supplemented state and residual vectors $\tilde{W}$ and $\tilde{R}$ are defined as

$$\tilde{W} = [x, \rho\Omega, \rho u\Omega, \rho e_t \Omega]^T \qquad \text{and} \qquad \tilde{R} = [-s, R]^T.$$

The residual vector appearing above is assembled using the time-averaged areas and midpoint grid velocities defined in Eqs. (19)–(21) and Eq. (9), respectively, as required by the GCL. For the 4-stage scheme the coefficients are taken to be

$$a_1 = \frac{1}{4}, \qquad a_2 = \frac{1}{3} \qquad a_3 = \frac{1}{2} \qquad a_4 = 1.$$

This choice of coefficients leads to a scheme which is fourth-order time accurate for a system of linear equations. It is stressed that the interface velocity, s, appearing in the supplemented residual vector and throughout the preceding development is arbitrary and ultimately user defined.

Recalling the eigenvalues of the ALE form, the Courant number, σ, is defined here as

$$\sigma = \max\left[\frac{(|\hat{u}| + c)}{\Delta x}\right]\Delta t. \tag{39}$$

BOUNDARY CONDITIONS

The nonlinear characteristic equations for the 1D Euler set in the absence of grid motion are

$$\frac{dp}{dt} \pm \rho c \frac{du}{dt} + \frac{n\rho u c^2}{x} = 0, \tag{40}$$

where the time derivative is the total time derivative along the $(u \pm c)$ characteristics given by

$$\frac{d}{dt} = \frac{\partial}{\partial t} + (u \pm c)\frac{\partial}{\partial x}. \tag{41}$$

In Eq. (40), n takes on the values 0, 1, and 2 for the Cartesian, cylindrical, and spherical coordinates, respectively [23]. A rigid wall perfectly reflecting boundary condition applicable to subsonic conditions can be constructed from Eq. (40), which has proven to perform reasonably well for the three coordinate systems considered here by simply neglecting the third term (which is singular at the origin of the cylindrical and spherical coordinate systems) in Eq. (40) and integrating the remaining terms.

For subsonic conditions $(u - c)$ is an outgoing wave at the left computational boundary and the wall boundary pressure p_w can be simply extracted from Eq. (40). In terms of an explicit m-stage scheme a purely reflecting condition at the left computational boundary is

$$p_w^{k+1} = p_i^k - (u\rho c)_i^k, \tag{42a}$$

where the subscript i denotes the cell centered value immediately adjacent to the wall. For purely reflecting subsonic conditions at the right computational boundary $(u + c)$ is an outgoing wave giving

$$p_w^{k+1} = p_i^k + (u\rho c)_i^k. \tag{42b}$$

This is the same prescription for the wall pressure used in [10] and is all that is needed to complete the boundary flux prescription at a rigid wall.

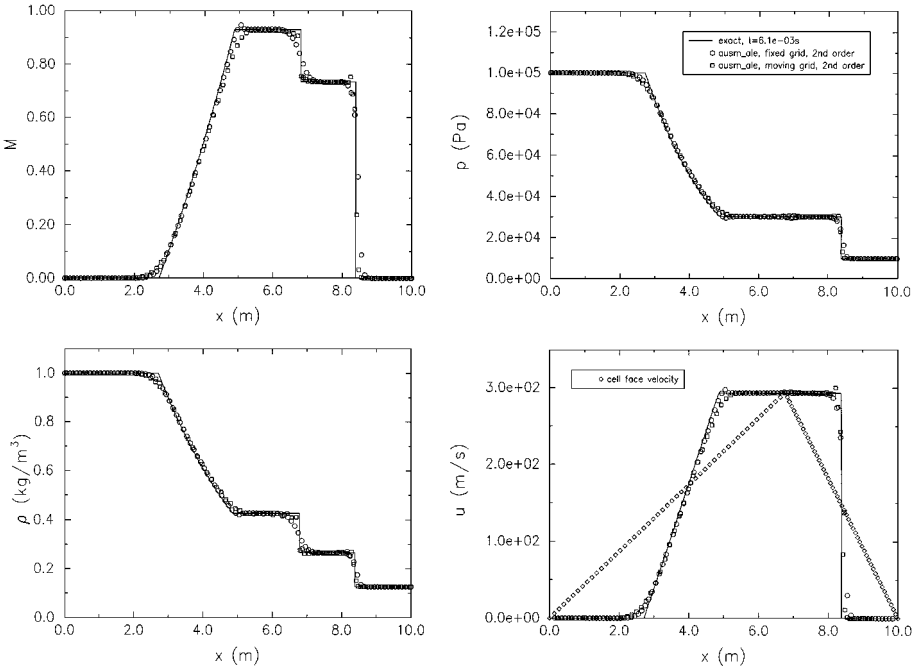

FIG. 3. Comparison of fixed and moving grid solutions for the shock tube problem (Sod).

BASIC TEST CASES

All computed results shown in this section were obtained using a 100-cell discretization and $\sigma = 0.5$. The ideal gas law is used as the EOS for the basic test cases and is given by

$$p = (\gamma - 1)\rho e. \tag{43}$$

Figure 3 compares the AUSM(ALE) solution with the exact solution for the Sod [24] shock tube problem ($\gamma = 1.4$). For this test case a Lagrangian surface is established at the contact discontinuity and the grid velocity is tapered linearly to zero at both ends of the computational domain, as shown in the figure. Both fixed and moving grid results are in good agreement with the exact solution for this case, although the contact is more sharply resolved by the moving grid method since the dissipation vanishes at the Lagrangian contact surface.

The infinite reflected shock problem ($\gamma = 5/3$) of Noh [25] is a particularly appropriate test case since exact solutions are available for the three coordinate systems investigated here. Figure 4 compares the AUSM(ALE) solution with the exact solution in Cartesian coordinates. The solution computed using the fixed grid bears little resemblance to the exact solution for this case. It should be recalled that AUSM(ALE) recovers exactly the U-split version of AUSM when the grid is fixed. Consequently, it may be concluded that the U-split version of AUSM performs very poorly for this test case. Difficulties with the basic AUSM scheme [9] when applied to reflected shock problems have been reported elsewhere [26].

The moving grid solution was generated by establishing a Lagrangian surface at the right computational boundary and linearly tapering the grid velocity to zero at the origin, as shown in the figure. With the moving grid the solution is correctly computed although

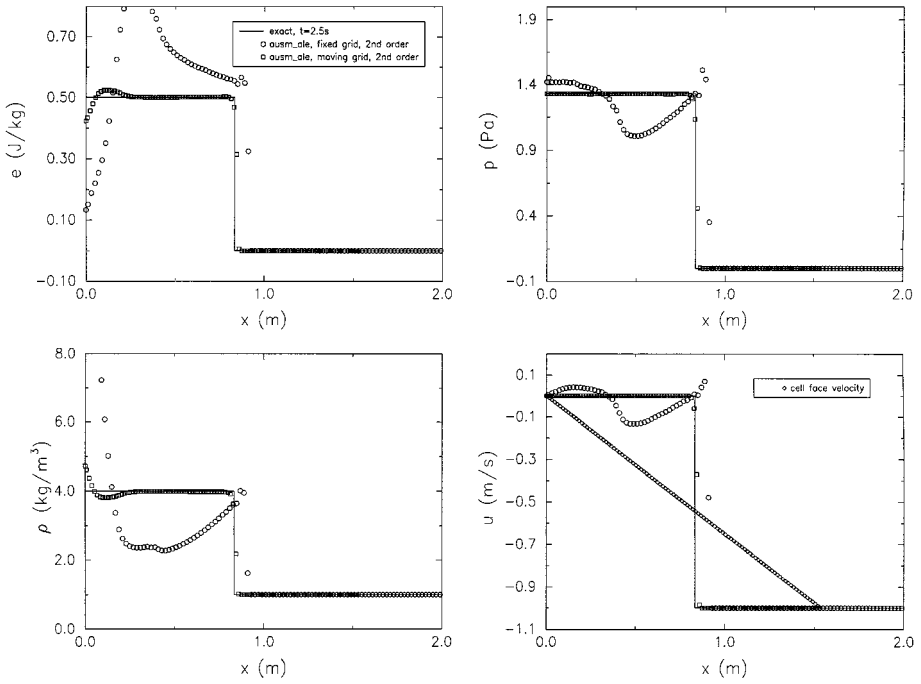

FIG. 4. Comparison of fixed and moving grid solutions for the infinite reflected shock problem (Cartesian case).

there is some underheating at the origin. The improved performance of the moving grid calculation may be attributable to two factors. First, the role of the nonlinear convection terms has been lessened since the grid is moving in the same direction as the fluid. Second, the grid motion compresses the grid points into the postshock region, resulting in higher resolution there. Results for the cylindrical and spherical coordinate systems are shown in Figs. 5 and 6.

In the cylindrical and spherical cases similar accuracy is achieved for both the fixed and moving grid computations, although the moving grid results are somewhat more diffusive compared to the fixed grid results. Also the overshoot at the shock has been eliminated with grid movement. The oscillations which are evident at the origin in the cylindrical and spherical cases may be associated with the singularity of the characteristic boundary condition, Eq. (40), at the origin of these coordinate systems. An investigation of the singularity of the boundary condition at the origin is beyond the scope of the present paper, although a refinement of the grid at the origin was found to eliminate the oscillations in Figs. 5 and 6.

APPLICATION TO A SPHERICALLY SYMMETRIC UNDERWATER EXPLOSION

To determine the utility of the method for multi-phase problems with strong shock and contact discontinuities AUSM(ALE) is applied to a benchmark 1D spherically symmetric underwater detonation problem. This problem has been investigated by several authors [27, 28] and a benchmark numerical solution is available [29]. The arbitrariness of the control surface motion that is available with the ALE form of the conservation laws is utilized in this problem to unambiguously maintain the boundary separating the gas and condensed phases of an underwater explosion.

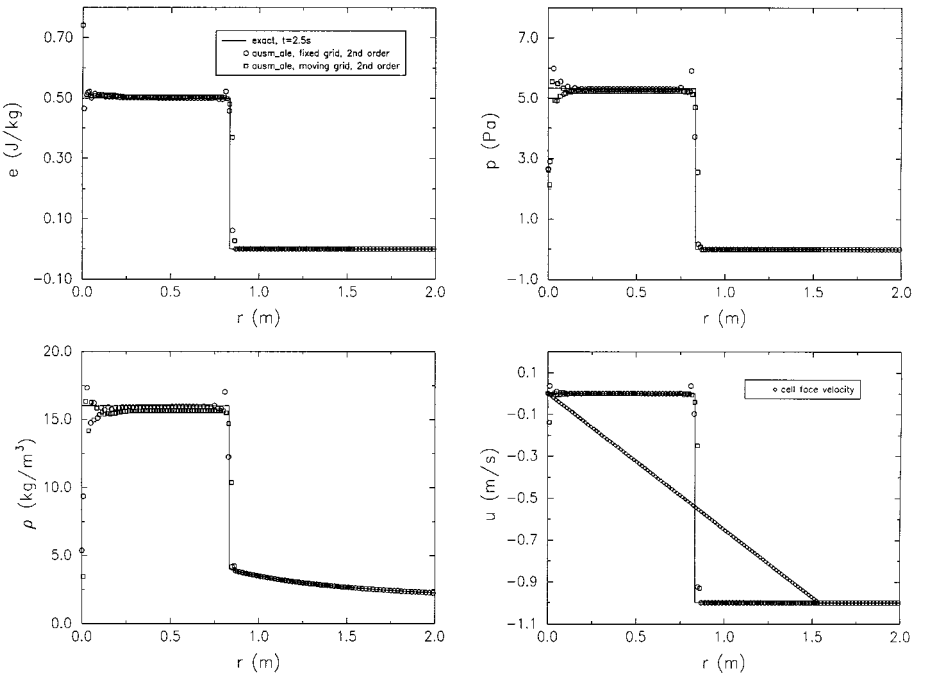

FIG. 5. Comparison of fixed and moving grid solutions for the infinite reflected shock problem (cylindrical case).

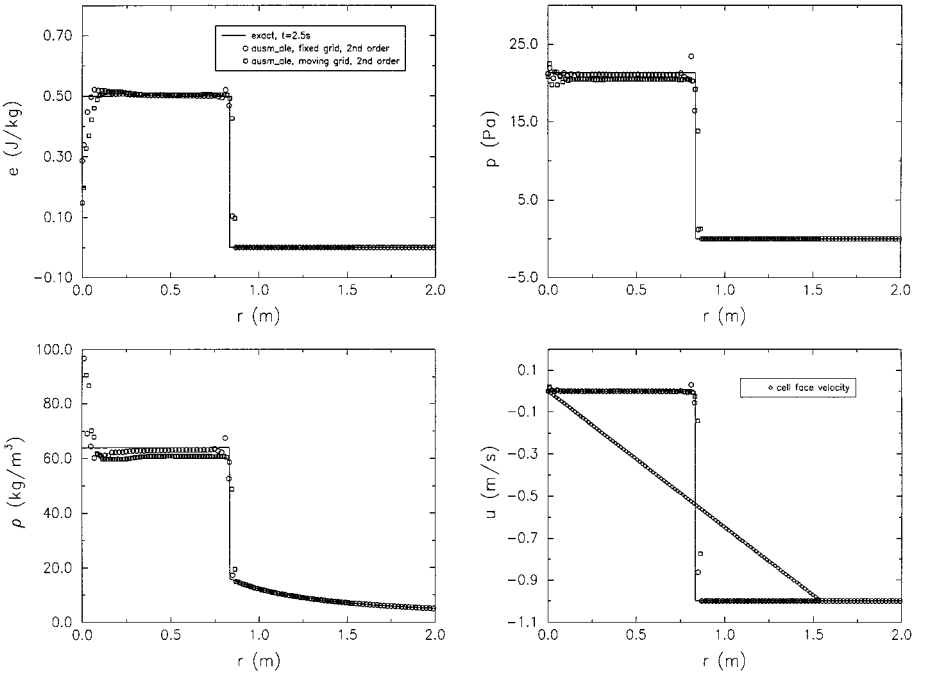

FIG. 6. Comparison of fixed and moving grid solutions for the infinite reflected shock problem (spherical case).

Since the problem is essentially a two-phase spherical analog to the classical shock tube problem the initial conditions (in SI units) are given using standard Riemann problem notation. The initial conditions are $[1.630(10^3), 0, 8.381(10^9)]_L$ and $[1.025(10^3), 0, 1.0(10^6)_R$ where the $[\rho, u, p]_L$ refers to the detonation-products phase and $[\rho, u, p]_R$ refers to the water phase. The charge is a 16-cm-radius TNT sphere. These are the same initial conditions used in the "uniform Euler" case of [29]. The Jones–Wilkins–Lee (JWL) EOS is used for the detonation-products gas [30] and an isentropic Tait relation for liquid water [31] is used. The specific state relationships are given by

$$p = A\left(1 - \frac{\omega\rho}{R_1\rho_0}\right)\exp^{-R_1\rho_0/\rho} + B\left(1 - \frac{\omega\rho}{R_2\rho_0}\right)\exp^{-R_2\rho_0/\rho} + \omega\rho e \qquad \text{(JWL)} \quad (44)$$

$$p = B\left(\left(\frac{\rho}{\rho_0}\right)^{\gamma} - 1\right) + A \qquad \text{(Tait)}. \quad (45)$$

The JWL constants for TNT are $A = 3.712(10^{11})$, $B = 3.230(10^9)$, $R_1 = 4.15$, $R_2 = 0.95$, $\omega = 0.30$, $\rho_0 = 1.630(10^3)$, $e_0 = 4.290(10^6)$. The Tait constants for water are $A = 1.0(10^5)$, $B = 3.31(10^8)$, $\rho_0 = 1.025(10^3)$, $\gamma = 7.15$.

The isentropic Tait equation for water does not involve internal energy and is consequently restricted to the liquid phase. When the Tait form is used the energy equation uncouples from the remaining conservation laws and a reduced Euler system governs the fluid dynamics. Other EOS have been used for water in underwater explosion studies [29].

The calculation was done using 600 cells in the detonation-products gas phase and the same number in the water phase with $\sigma = 0.5$. A Lagrangian surface is established at the material and phase interface by constraining the grid velocity to match the fluid velocity at the interface. The grid velocity is further constrained to match the primary shock wave speed at the outer boundary of the domain and to be zero at the origin. At intermediate points between these constraints the grid velocity is linearly interpolated. This arrangement maintains the material separation of the liquid and gas phases and ensures that all grid points participate in the resolution of the flow field as the primary shock wave propagates outward. The phase boundary is indicated in Figs. 7–9 by the open square symbol in the pressure profiles.

As shown in Fig. 7 the initial phase of the detonation begins with the primary shock wave moving to the right into undisturbed ambient fluid and an expansion wave moving to the left toward the origin. The expansion wave reflects from the origin as an expansion resulting in a region of very low pressure near the origin. The outward inertia of the expanding gas is eventually overcome by the centripetal pressure gradient and the gas reverses direction, forming an inward moving shock wave which in turn reflects as a shock from the origin. This reflected secondary shock wave then propagates outward toward the water interface. The flow in the gas phase becomes supersonic during this phase of the detonation, as shown in the figure.

Figure 8 shows the secondary shock wave arriving at the gas/water interface and subsequently being partially transmitted to the water phase and partially reflected back into the gas phase. The reflected portion is again reflected from the origin, resulting in a tertiary outward moving shock which again will be partially transmitted and partially reflected at the interface. This process repeats numerous times, each time at a reduced shock strength, as shown in Fig. 9. The primary, secondary, and tertiary waves can be seen most clearly in the pressure profiles of Figs. 8 and 9.

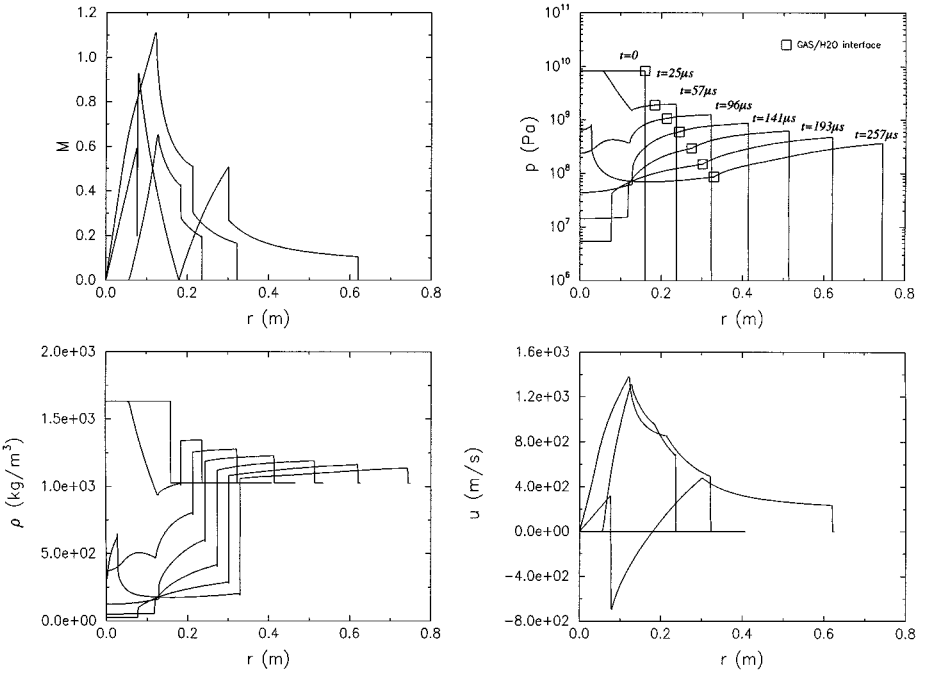

FIG. 7. Initial phase of spherically symmetric underwater explosion problem.

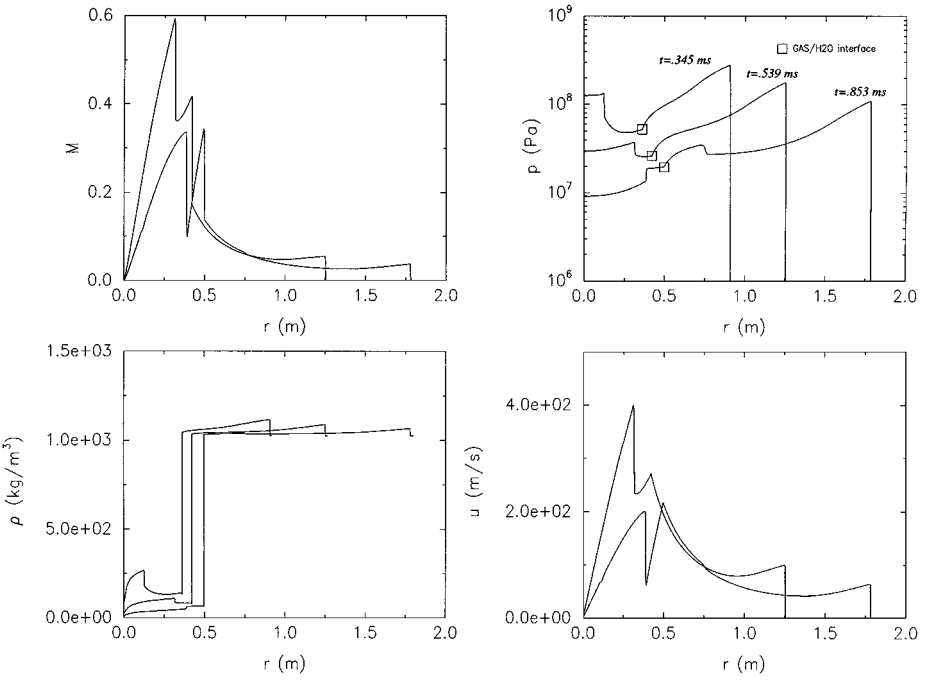

FIG. 8. Shock/free-surface interaction phase of spherically symmetric underwater explosion problem.

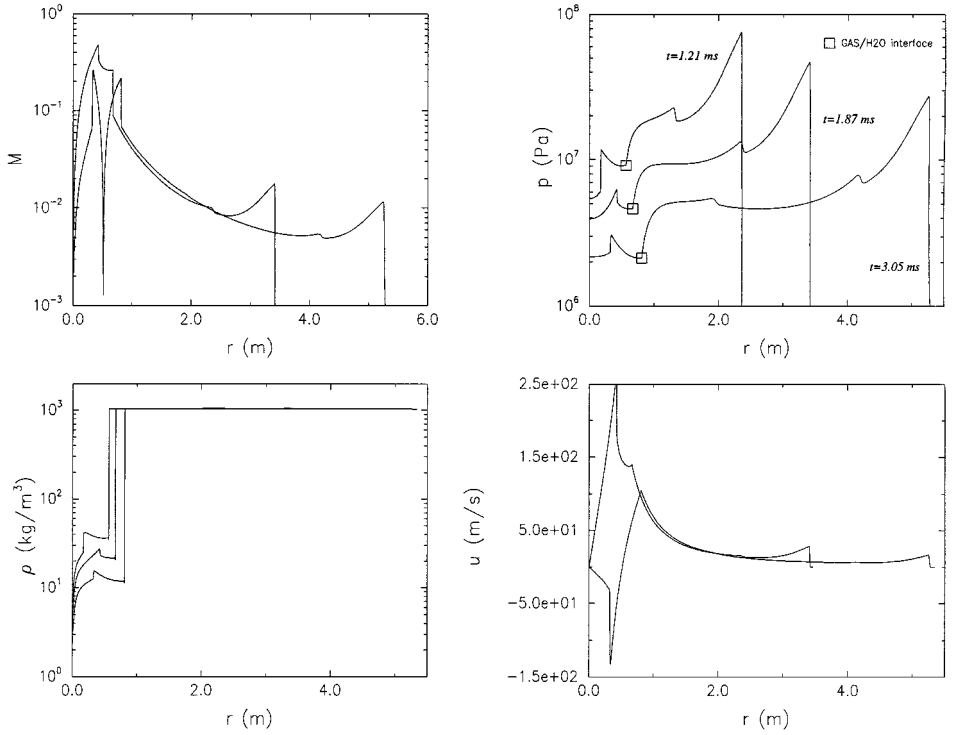

FIG. 9. Incompressible phase of spherically symmetric underwater explosion problem.

By the time the primary shock wave has traveled approximately 50 charge radii the pressure within the expanding gas bubble has dropped well below the ambient pressure. The centripetal pressure gradient gradually halts the expansion of the detonation-products gas bubble, which ultimately reverses its expansion and enters the collapse phase. Computed results using AUSM(ALE) indicate the bubble reaches a maximum radius of 2.19 m at $t = 65.8$ ms. These results are within 1% of the benchmark values reported in [29] using a two-step Lagrange plus remap Godunov scheme. The Mach number is typically less than 10^{-1} during this phase of the detonation event, as shown in Fig. 9, and the flow is essentially incompressible.

CONCLUSIONS

The ALE version of AUSM presented here when used in conjunction with a geometrically conservative prescription for time-dependent control surface areas offers an accurate and robust method for capturing strong shock, contact, and phase discontinuities on arbitrarily moving grids. Although the development given here was limited to 1D the extension to multi-dimensions is relatively straightforward using either a general coordinate transformation of a logically connected rectangular grid or an unstructured finite volume mesh. The splitting of flux components based on the eigenvalues of the ALE form and the introduction of a common sound speed at a Lagrangian surface greatly facilitate accurate shock capturing in the presence of grid movement. The utility of arbitrarily introducing a Lagrangian surface into the computational domain was demonstrated in the two-phase

underwater detonation problem where the establishment of a Lagrangian surface ensured the unambiguous separation of water and gas phases during the calculation. The compelling features of the method are its simplicity and the ease with which real fluid state relations can be accommodated. Finally, the method is shown to recover exactly the U-split version of AUSM in the absence of grid motion.

ACKNOWLEDGMENTS

The author acknowledges the support provided by the Internal Research Program at the Coastal System Station, Naval Surface Warfare Center, Dahlgren Division. He also thanks Dr. M. S. Liou at NASA Lewis Research Center for his guidance and suggestions regarding the AUSM family of schemes.

REFERENCES

1. T. Nomura and T. J. R. Hughes, An arbitrary Lagrangian–Eulerian finite element method for interaction of fluid and a rigid body, *Comput. Methods Appl. Mech. Engrg.* **95**, 115 (1992).
2. W. Shyy, H. S. Udaykumar, M. M. Rao, and R. W. Smith, *Computational Fluid Dynamics with Moving Boundaries* (Taylor and Francis, Washington, DC, 1996).
3. W. G. Szymczak, J. C. W. Rogers, J. M. Solomon, and A. E. Berger, A numerical algorithm for hydrodynamic free boundary problems, *J. Comput. Phys.* **106**, 319 (1993).
4. R. Lohner, C. Yang, J. Cebral, and J. D. Baum, Fluid–structure interaction using a loose coupling algorithm and adaptive unstructured grids, in *Computational Fluid Dynamics Review* (Wiley, Sons, New York, 1995).
5. C. W. Hirt, A. A. Amsden, and H. K. Cook, An arbitrary Lagrangian–Eulerian computing method for all flow speeds, *J. Comput. Phys.* **14**, 227 (1974).
6. C. Hirsch, *Numerical Computation of Internal and External Flows* (Wiley, New York, 1988), Vol. 2, p. 408.
7. P. L. Roe, Approximate Riemann solvers, parameter vectors and difference schemes, *J. Comput. Phys.* **43**, 357 (1981).
8. B. Van Leer, Flux vector splitting for the Euler equations, *Lecture Notes Phys.* **170**, 507 (1982).
9. M. S. Liou and C. J. Steffen, A new flux splitting scheme, *J. Comput. Phys.* **107**, 23 (1993).
10. M. S. Liou, A sequel to AUSM: AUSM$^+$, *J. Comput. Phys.* **129**, 364 (1996).
11. Y. Wada and M. S. Liou, An accurate and robust flux splitting scheme for shock and contact discontinuities, *SIAM J. Sci. Comput.* **18**, 633 (1997).
12. J. Y. Trepanier, M. Reggio, H. Zhang, and R. Camarero, A finite-volume method for the Euler equations on arbitrary Lagrangian–Eulerian grids, *Comput. Fluids* **20**, 399 (1991).
13. C. Hirsch, *Numerical Computation of Internal and External Flows* (Wiley, New York, 1988), Vol. 1, p. 24.
14. V. Venkatakrishnan, Perspective on unstructured grid flow solvers, *AIAA J.* **34**, 533 (1996).
15. P. D. Thomas and C. K. Lombard, Geometric conservation law and its application to flow computations on a moving grid, *AIAA J.* **17**, 1030 (1979).
16. H. Zhang, M. Reggio, J. Y. Trepanier, and R. Camaero, Discrete form of the GCL for moving meshes and its implementation in CFD schemes, *Comput. Fluids* **22**, 9 (1993).
17. B. Nkonga and H. Guillard, Godunov-type method on non-structured meshes for three-dimensional moving boundary problems, *Comput. Methods Appl. Mech. Engrg.* **113**, 183 (1994).
18. M. Lesoinne and C. Farhat, Geometric conservation laws for flow problems with moving boundaries and deformable meshes, and their impact of aeroelastic computations, *Comput. Methods Appl. Mech. Engrg.* **134**, 71 (1996).
19. S. K. Godunov, A finite difference method for for the numerical computation of discontinuous solutions of the equations fluid dynamics, *Math. Sb.* **47**, 375 (1959).
20. M. S. Liou, B. Van Leer, and J. S. Shuen, Splitting of inviscid fluxes for real gases, *J. Comput. Phys.* **87**, 1 (1990).

21. D. Darracq, S. Champagneux, and A. Corjon, Computation of unsteady turbulent airfoil flows with an aeroelastic AUSM$^+$ implicit solver, AIAA Paper 98-2411, in *16th AIAA Applied Aerodynamics Conference* (1998).
22. B. Van Leer, C. H. Tai, and K. G. Powell, Design of optimally smoothing multi-stage schemes for the Euler equations, AIAA Paper 89-1933, in *9th AIAA Computational Fluid Dynamics Conference* (1989).
23. K. W. Thompson, Time dependent boundary conditions for hyperbolic systems, *J. Comput. Phys.* **68**, 1 (1987).
24. G. A. Sod, A survey of several finite difference methods for systems of nonlinear hyperbolic conservation laws, *J. Comput. Phys.* **27**, 1 (1978).
25. W. F. Noh, *Artificial Viscosity (Q) and Artificial Flux (H) Errors for Spherically Divergent Shocks* (Lawrence Livermore National Laboratory, 1983).
26. L. Bergamini and P. Cinnella, A comparison of 'new' and 'old' flux-splitting schemes for the Euler equations, AIAA Paper 93-0876, in *31th AIAA Aerospace Sciences Meeting* (1993).
27. L. D. Landau and E. M. Lifshitz, *Fluid Mechanics* (Pergamon Press, London, 1959), p. 392.
28. J. Flores and M. Holt, Glimm's method applied to underwater explosions, *J. Comput. Phys.* **44**, 377 (1981).
29. A. B. Wardlaw and H. Mair, Spherical solutions of an underwater explosion bubble, one-dimensional benchmark solutions for underwater explosion bubble simulations, *Shock and Vibration* **5**, 89 (1998).
30. B. M. Dobratz and P. C. Crawford, *LLNL Explosives Handbook—Properties of Chemical Explosives and Explosive Simulants* (Lawrence Livermore National Laboratory, 1985).
31. R. H. Cole, *Underwater Explosions* (Dover, New York, 1948), p. 36.